Saudi Journal of Biological Sciences 28 (2021) 2128–2138

Contents lists available at ScienceDirect

Saudi Journal of Biological Sciences

journal homepage: www.sciencedirect.com

Original article

Structural insight into mutations at 155 position of valosin containing protein (VCP) linked to inclusion body myopathy with Paget disease of bone and frontotemporal Dementia

Rui Wu *, Zhijie Wei, Li Zhang

Department of Neurology, Affiliated Hospital of Zunyi Medical University, Zunyi, Guizhou 563000, China

ARTICLE INFO

Article history:
Received 19 November 2020
Revised 10 February 2021
Accepted 11 February 2021
Available online 19 February 2021

Keywords:
Valosin-containing protein
Myopathy
Paget disease
Dementia
Molecular docking

ABSTRACT

Mutations in *Valosin-containing protein (VCP)* have been implicated in the pathology linked to inclusion body myopathy, paget disease of bone and frontotemporal dementia (IBMPFD). VCP is an essential component of AAA-ATPase superfamily involved in various cellular functions. Advanced *In-silico* analysis was performed using prediction based servers to determine the most deleterious mutation. Molecular dynamics simulation was used to study the protein dynamics at atomic level. Molecular docking was used to study the effect of mutation on ATP/ADP transition in the kinase domain. This ATPase of 806 amino acids has four domains: N-terminal domain, C-terminal domain and two ATPase domains D1 and D2 and each of these domains have a distinct role in its functioning. The mutations in VCP protein are distributed among regions known as hotspots, one such hotspot is codon 155. Three missense mutations reported in this hotspot are R155C, R155H and R155P. Potentiality of the deleteriousness calculated using server based prediction models reveal R155C mutation to be the most deleterious. The atomic insight into the effect of mutation by molecular dynamics simulation revealed major conformational changes in R155C variants ATP binding site in D1 domain. The nucleotide-binding mode at the catalytic pocket of VCP and its three variants at codon 155 showed change in the structure, which affects the ATP–ADP transition kinetics in all the three variants.

1. Introduction

Frontotemporal Dementia (FTD) formerly known as "Picks Disease" is an anomaly of neurodegenerative disorder caused by neuronal loss in frontal and/or temporal lobes of the brain (Lowe and Spillantini, 1998). The disease features gradual and progressive decline in behaviour and/or language, based on these signs FTD is divided into two major clinical syndromes: the behavioural variant and the language variant (Rascovsky et al., 2011). With almost equal incidence has been reported in men and women, the signs and symptoms of FTD become evident more commonly between the age group of 45 and 65 years. This disease is most prevalence like Alzheimer's disease and limited studies have shown a trend of 20–50% of reported cases younger than 65 years (Ratnavalli et al., 2002). The aetiology of FTD has been associated with mutations. Mutations in MAPT, GRN, TARDBP, CHMP2B and VCP genes are known genetic factors for aetiology of FTD (Lynch et al., 1994; Baker et al., 2006; Van Swieten and Heutink, 2008; Kabashi et al., 2008; Skibinski et al., 2005; Neumann et al., 2007).

Mutations in *valosin-containing protein* (*VCP*) gene are associated with inclusion body myopathy and Paget disease of bone and FTD (IBMPFD), which is a rare autosomal-dominant disorder (Neumann et al., 2007; Watts et al., 2004). The disease is characterized by adult-onset proximal and distal muscle weakness, early-onset of Paget disease of bone (PDB) in most cases, and premature FTD (Kovach et al., 2001). PDB involves increased bone turnover, localized enlargement with deformity of the long bones. Early stages FTD in IBMPFD patients is characterized by progressive decline in behaviour by showing traits like dysnomia, paraphasic errors, comprehension deficits, dyscalculia and memory loss. In advanced stage of FTD language disability, alexia, and agraphia become evident. Among individuals who meet diagnostic criteria

* Corresponding author: Department of Neurology, Affiliated Hospital of Zunyi Medical University, No. 149, Dalian Road, Huichuan District, Zunyi, Guizhou 563000, China.
E-mail address: lwwzj@163.com (R. Wu).

Peer review under responsibility of King Saud University.

Production and hosting by Elsevier

https://doi.org/10.1016/j.sjbs.2021.02.048
1319-562X/

for IBMPFD, nearly 100% have an identified mutation in the *VCP-gene*, and approximately 80% of individuals have family history and 20% are first time affected by *de-novo* mutations (Kimonis et al., 2018).

VCP protein is an essential component of AAA-ATPase superfamily involved in cell cycle regulation (Hetzer et al., 2001), homotypic membrane fusion (Kondo et al., 1997), postmitotic Golgi reassembly (Rabouille et al., 1998) and ubiquitin–proteasome pathway-mediated endoplasmic reticulum-associated degradation (Watts et al., 2004). The VCP protein is an ATPase constituting of 806 amino-acids, the protein has four domains: N-terminal domain, C-terminal domain and two ATPase domains D1 and D2. The N-terminal domain binds specific ubiquitin substrates through cofactors such as Ufd1, Npl4, and p47 and the C-terminal domain binds multiubiquitination enzyme Ufd2 (Wang et al., 2004). Till date ten VCP missense mutations has been reported and half of which fall in mutation hotspots (Kimonis et al., 2008). One such hotspot is codon 155, where a missense mutation is a cause of IBMPFD in more than 50% of reported IBMPFD individuals. The three missense mutations reported in this hotspot are R155C (Guyant-Marechal et al., 2006), R155H (Viassolo et al., 2008) and R155P (Haubenberger et al., 2005), among them R155H is the most common.

To understand the effect of single amino acid substitution on protein structure and dynamics, the use of *In-silico* techniques has become a reliable tool (Mokhdomi et al., 2016). In this study we have used computer aided prediction methods to evaluate the damaging capability of the mutations. VCP protein and its 155 codon variants we observed under virtual microscope of molecular dynamics simulation, the tool is used to observe the conformational changes inflicted by the mutation on protein structure.

2. Material and methods

2.1. Data set preparation

The atomic coordinates of a single monomer VCP protein used in this study were retrieved from PDB entry: 4KLN (Tang and Xia, 2013), the coordinated amino acids alone were used to generate the models using mutate module of Discovery Studio 4.5 (Studio, 2013). The X-ray crystallographic structure was the highest resolved (2.62 Å) structure available for a hexameric assembly. The geometry of the modelled structures was optimized using Swiss PDB viewer, where the structures were searched for missing atoms and energy was minimized. The first structure generated was Wt, and GROMACS 4.6.5 (Pronk et al., 2013) platform was used for energy minimization. The other three structures generated from Wt were Mu1 (R155C), Mu2 (R155H) and Mu3 (R155P). The same nomenclature was used throughout the study. The ATP and ADP structures used for molecular docking analysis were retrieved from PubChem database. All the simulations in this study were carried out using GROMOS 43a1 force field.

2.2. SNP damage prediction

The deleterious effect of the mutations was studied using prediction based models. Three online servers selected were SIFT (Kumar et al., 2009), PolyPhen2 (Adzhubei et al., 2010) and PoPMuSiC (Dehouck et al., 2011).

2.3. Molecular dynamics simulation

Molecular dynamics simulation using GROMACS 4.6.5 platform (Pronk et al., 2013) was used to look into the dynamics of the VCP and its three 155 codon variants. 50 ns simulation of native and mutant proteins was carried out. The proteins were placed in water with simple point charge (SPC) water molecule and ions (Jorgensen et al., 1983). The ions were added using the GENION tool of the GROMACS, the random water molecules were replaced by Na^+ or Cl^- ions to achieve the simulation under physiological salt concentration (150 mM). Periodic boundary condition were set to maintain constant pressure and temperature, Parrinello-Rahman method and Berendsen temperature coupling method were were employed for pressure and temperature, respectively (Berendsen et al., 1984; Martoňák et al., 2003). Position restrain simulation was performed at 310 K for 1 ns with a coupling time of 0.2 ps. The bond formation was regulated by SHAKE algorithm, which was used to impose general harmonic constraints after every two frames during molecular simulations (Elber et al., 2011). A final

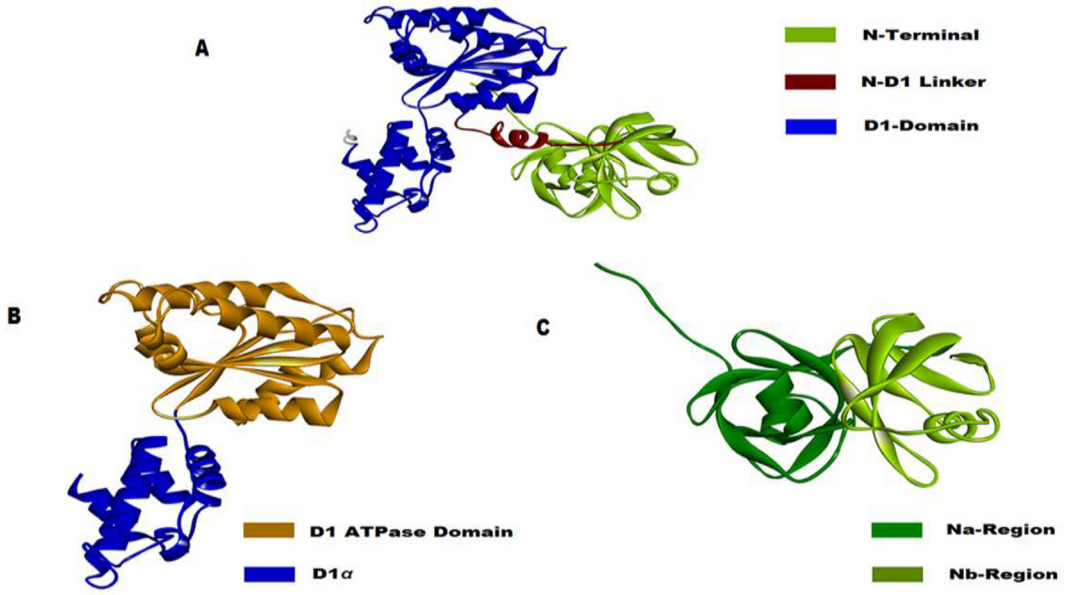

Fig. 1. Systematic representation of domains and sub-domains of valosin-containing protein, the subdomains have been color marked.

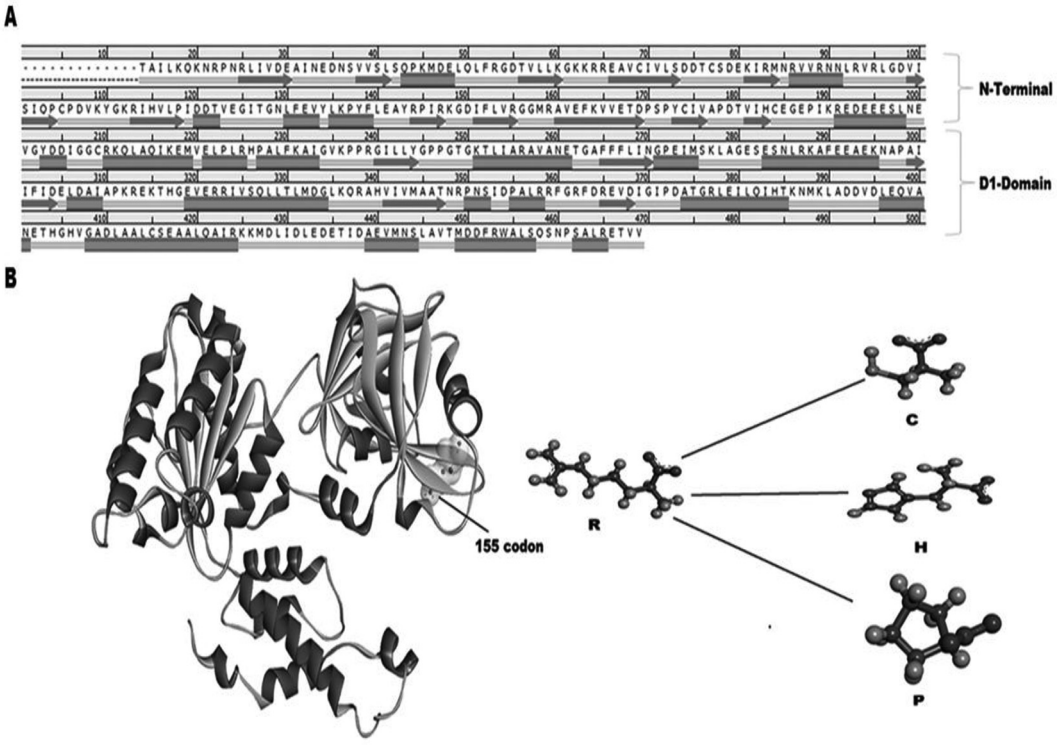

Fig. 2. (A) Average secondary structure of the VCP domains under investigation shown in 2d representation. (B) The structure of vasolin containg protein showing codon 155 and its variants.

run of 50 ns was performed; the trajectories generated were analysed using GROMACS in-build tool. DSSP program was used to check the secondary structure architecture over time (Hooft et al., 1996). Graphs were plotted using Grace and GNUPLOT programs (Turner, 2005; Racine, 2006). All the visualizations were carried out using pymol and discover studio visualize (DeLano, 2002).

2.4. Molecular docking simulation and MM-PBSA calculations

AutoDock 4.2 tool (Goodsell et al., 1996) was used for molecular docking simulations, ATP and ADP were alternatively used to evaluate the nucleotide-binding mode at the catalytic pocket of VCP and its three variants at codon 155.

3. Results

3.1. Structure and assembly of VCP protein

Schematic representation of the domains and sub-domains were shown in Fig. 1, the portion of the VCP protein under investigation ranges from 14 to 469 amino acids and can be divided into N-terminal (14–187) and D1-domain (209–460) with N-terminal and D1-domain linker ranging from 188 to 208. The N-terminal region has two sub-domains of Na and Nb required for cofactor and substrate binding. The D1-Domain has two regions D1-ATPase domain (209–370) and D1α domain (370–460). The D1-ATPase domain has three sub-domains Walker A motif (WA), Walker B motif (WB) and second region of homology (SRH).

Fig. 2(A) shows the secondary structure architecture of the domains and the sub-domains, Fig. 2(B) shows the crystallographic structure of the two domains and the 155 codon position and its variant amino acids. The amino acid arginine has its own specific size, charge, hydrophobic value and the three variants differ in these properties. The mu1 has R155C variation, the variant cysteine is smaller in size, neutral in charge and changes the five running hydrophobicity value (Fig. 3). Mu2 R155H variation, the change in five running hydrophopicity value is least, but the change in charge and size at 155 position due to incorporation of histidine. The variation at 155 codon under observation is of R155P, where proline incorporation changes the size and charge of the position, however change in five running hydophobicity is least. The change in the amino-acid properties is a factor that may alter the phenomenon of asymmetry in hexameric structure of VCP proteins, this change can alter the functioning, particularly the ATP/ADP transition.

3.2. Prediction based mutational analysis

Three *in-silico* tools were selected for predicting the damaged effect of the mutation, the selection of the servers was done to check both sequence and structure based effect. For SNP damage prediction *in-silico* tools use algorithms that have been outlined, designed, and developed for predicting whether a mutation is deleterious or neutral. These uses of such tools make studies more feasible and accurate and are less time-consuming. The selected servers for this study looked into and double checked both sequence and structure based effect of the selected mutations. Table 1 shows the result generated, selected servers predicted all the three mutations to be damaging (see Tables 2–5).

For sequence based method to predict the effect of mutations at codon 155, used SIFT server and the three mutations were classified as damaging and tolerated, mu1 was predicted to be damaging among the three. PolyPhen2 (Polymorphism Phenotyping v2) is a tool which predicts possible impact of an amino acid substitution on the structure and function of a human protein using straight forward physical and comparative considerations. In this HumDiv (a preferred model for evaluating rare alleles) predicted all the mutation to be PROBABLY DAMAGING, R155C is the most damag-

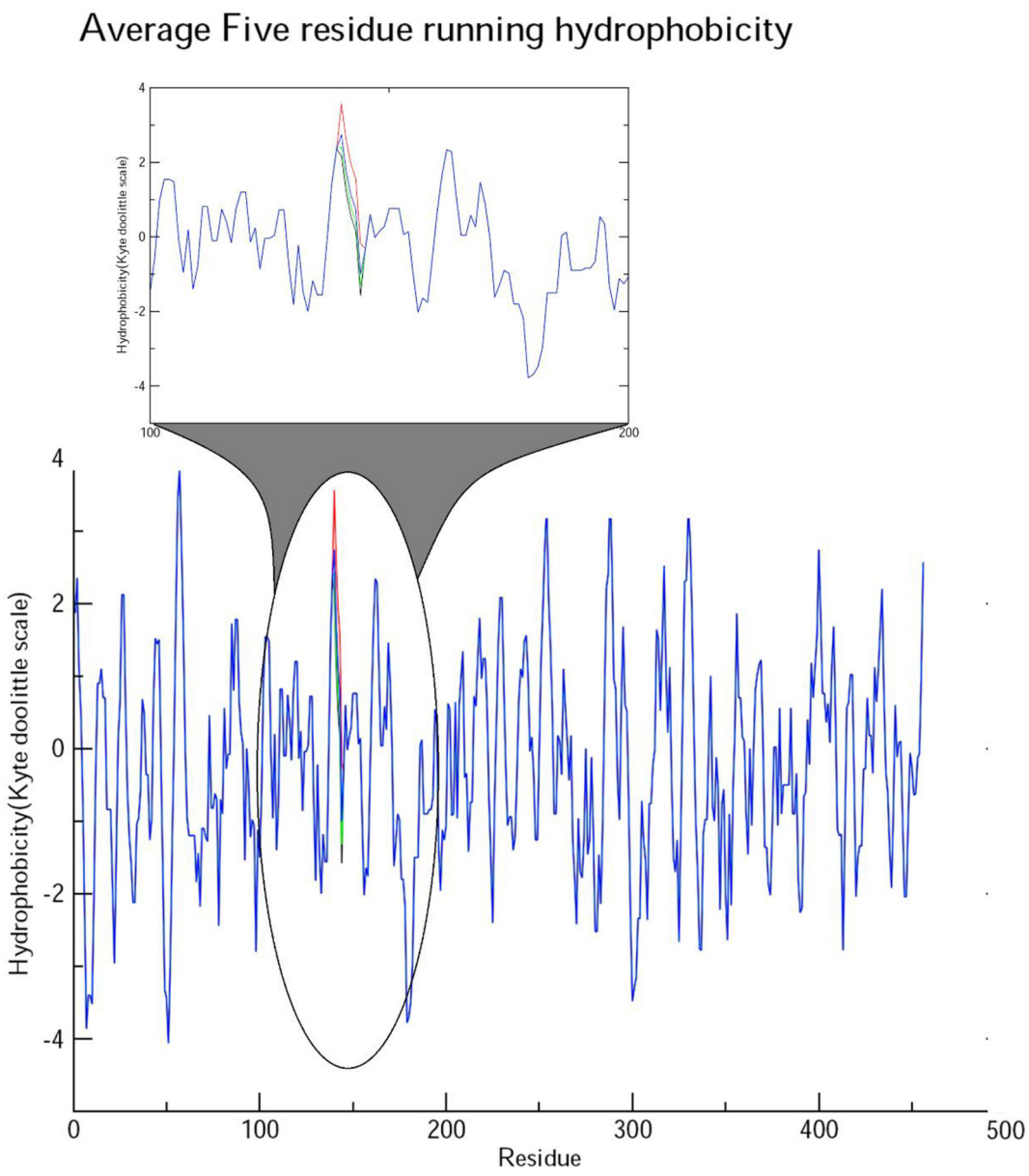

Fig. 3. Graphical representation of variation in hydrophobicity observed using kyte-doolittle scale. Single amino acid substitution at 155codon shows considerable change in average five running hydrophobicity.

ing of the three with a score of 1 (sensitivity: 0.00; specificity: 1.00) as shown in Fig. 4(A). Other model i.e. HumVar (a preferred model for diagnostic of Medalian Disease) predicted R155C and R155P to be PROBABLY DAMAGING and R155H as BENIGN - with a score of 0.135 (sensitivity: 0.90; specificity: 0.71) as shown in Fig. 4(B). The third tool that was used is PoPMuSiC, a tool for the CAD (computer aided design) of mutant proteins with controlled stability properties. It assess the changes in stability of a given protein or peptide under single-site mutation, on the basis of its structure. In this case single option was used that enabled to predict stability change resulting from a given mutations. The result generated showed R155C to be the most destabilizing with Acc = 75.50% and ΔG = 0.30 kcal/mol. The generated result showed R155C as highly deleterious and least stable.

Table 1
Summary of damage prediction score of online servers used.

Server	R155C	R155H	R155P
SIFT	DAMAGING	TOLERATED	TOLERATED
PolyPhen2	Probably damaging	Probably damaging	Probably damaging
PoPMuSiC	Destabilizing	Destabilizing	Destabilizing

3.3. Structural and conformational dynamics of VCP and its variants

The changes at 10 ns interval of time were taken and the picturesque representation is shown in Fig. 5. The results give a general outline of the effect of the mutations on protein structure and dynamics. To look into more detail, the average secondary structure layout was observed (Fig. 6). The mutation in the N-terminal region of VCP is changing the secondary structure layout of both N-terminal and D1-domain in all mutant structures. GROMACS inbuild tools g_rms, g_gyrate, g_sas and g_hbond tool were used to study the structural and conformational dynamics of VCP and its three 155 codon variants. Root mean square deviation (RMSD) was calculated using g_rms tool, Fig. 7(A) shows the value curves

Table 2
The ATP/ADP binding mode of the wildtype (wt), mutant1 (Mu1), mutant2 (Mu2) and mutant3 (Mu3) valosin-containing protein (VCP). Bold amino acida are common in ATP and ADP binding pockets.

	ATP Binding Mode	ADP Binding Mode
Wt	**ASN348**, PRO247, LYS251, **PRO 246**, THR249, GLY250, THR252, GLY248, ALA409, LEU253, ARG256, VAL201, HIS384, ALA412	PRO372, GLY208, GLN212, ILE369, GLY370, TYR244, **PRO246**, **ASN348**, ARG349, PRO350, ASN351, GLY245, ILE371, ASP 368
Mu1	**PRO247**, **PRO246**, **THR249**, **LYS251**, THR252, **LEU253**, **ALA409**, **ALA412**, **HIS384**, **GLY408**, **GLY248**, **GLY250**, **ASN348**	**PRO247**, **ASN348**, **PRO246**, **GLY248**, ASP205, **ALA409**, **THR249**, ILE380, ILE206, GLY207, PRO372, **GLY408**, **HIS384**, **LEU253**, **GLY250**, **ALA412**, THR252, **LYS251**, GLY305
Mu2	PRO372, **CYS209**, GLN212, GLY370, ILE371, ASP373, ILE369, GLY376, GLY208, **GLY250**, **ILE383**, **LEU253**, **ASP205**, **HIS384**, **GLY408**, **ALA412**, **ALA409**, **ILE206**, **ILE380**, **THR249**, LEU411, **GLY248**, **GLY207**	ASP304, ASN348, THR252, **GLY250**, **ALA409**, **HIS384**, **ALA412**, **ILE380**, **ASP205**, **ILE383**, **GLY207**, **ILE206**, **CYS209**, **THR249**, **LEU253**, THR347, GLU305, **GLY248**, LYS251, **GLY408**, PRO247
Mu3	**THR252, ALA409, LEU253, GLY248, LYS251, GLY250**, ILE383, **ILE206**, ILE254, **ILE369**, **GLN212**, **CYS209**, **THR249**, ASP205, **GLY207**, LEU211, **HIS384**, **GLY408**	**ALA409, THR252, LEU253, LYS251, GLY248, GLY250**, ILE380, **GLY408**, **ILE206**, LEU411, VAL407, PRO372, GLY208, **CYS209**, ILE371, GLY370, **GLN212**, **ILE369**, **THR249**, **GLY207**, **HIS384**, ALA412

Table3
Comparative Binding energy during ATP-ADP transition.

	Wt	R155C	R155H	R155P
ΔG_{ATP}	−9.63	−4.21	−7.31	−8.23
ΔG_{ADP}	−6.21	−6.71	−7.55	−7.21
$-\Delta G_{ATP/ADP}$	1.55	0.62	0.96	1.14

of wildtype and its mutant systems over time. Mu1 structure showed the maximum deviation, the deviation can be the result of change in secondary structure architecture. The RMSD result at 310 K temperature shows the wild type to converge at 0.5 nm at the end of the 50 ns simulation, the Mu1 modelled is showing the maximum deviation and at the end of the simulation the RMSD score is 0.8 nm. The RMSD graph is indicating wt, mu2 and mu3 structures reaming steady throughout 50 ns simulation. g_gyrate tools was used to check the effect of the mutation on radius of gyration (Rg)of the protein over time (Fig. 7B). The results show that all three mutant structure have slightly compact structure

Table 5
MM-PBSA calculations.

Summary	Wt	R155C	R155H	R155P
ATP Binding energy kJ/mol	−236.345 ±25.657	−163.901 ±32.714	−173.543 ±22.743	−201.154 ±25.387
ADP Binding energy kJ/mol	−182.634 ±23.873	−158.654 ±34.234	−145.567 ±31.565	−189.675 ±31.265

than wild type, at the end of 50 ns simulation mu1 structure is most compact with Rg of 2.45 nm. g_sas tool was used to calculate solvent accessible surface area (SASA) over time for hydrophobic as well as total residues of the four structures under observation. The SASA graph (Fig. 7C) shows decrease in SASA as the overall trend, the wildtype structure shows maximum area at 135 nm^2 after 50 ns simulation, while mu3 is showing the least SASA (125 nm^2) after 50 ns .

The hydrogen bond pattern was studied using g_hbond tool, intra-protein hydrogen bond pattern and protein water hydrogen bond pattern was studied. Fig. 8 shows the results generated the Wt VCP domain forms 336 average number of intra hydrogen bond per frame (each frame calculated after 2 ps) and with water the number is 917 hydrogen bond per frame. On comparison all the three mutant structures are showing decrease in average number of intra hydrogen bond per frame, the numbers are 328, 334 and 331 respectively for mu1, mu2 and mu3. The protein-water hydrogen bond pattern is also showing decrease in number as compared to wt. The mu1 structure is showing the least number 907 average number of intra hydrogen bond per frame. The change in intra hydrogen bond pattern could be a reason for secondary structure change observed in all three variants.

3.4. Flexibility and compactness in WT and mutants

To look into the flexibility and compactness of VCP N-terminal and D1 domain, g_rmsf tool of GROMACS package was employed. The tool calculates root mean square fluctuation (RMSF), giving an account of standard deviation of c-alpha atoms in the trajectory after fitting to a reference fame. Fig. 9 (A) represents the mobility of c-alpha atoms of the amino-acids, to investigate further the RMSF plot was broken into three, based on the structural domains of the VCP protein segment under investigation, Fig. 9(B) shows the RMSF plot of N-terminal, N-D1 linker and D1-Domain. The ATP binding domain of the D1-ATPase domain was studied for fluctuations, Fig. 9(C) shows the fluctuations. On observing the RMSF pattern it is evident that all the mutations have distinct fluctuation pattern. In r_rmsf tool the option -oq was used to convert the RMSF value into B Factor values and implicit them on the VCP structure

Table 4
The xyz coordinates of the amino acids selected for gauging the distance spanning in the ATP/ADP binding pocket.

		0 ns						50 ns					
	AA	X	Y	Z	Distance S197-G273	Distance G273-S416	Distance S416-S197	X	Y	Z	Distance S197-G273	Distance G273-S416	Distance S416-S197
Wt	SER197	34.6946	53.4539	43.4089				31.7779	53.7001	37.6851			
	GLU273	39.5023	55.981	52.556	23.355	27.645	**21.126**	39.1034	55.8395	52.419	27.791	28.609	**33.077**
	SER416	40.0235	43.6928	46.1828				40.6622	44.9388	43.1943			
Mu1	SER197	34.7196	53.2642	43.4592				38.4605	56.2085	49.1635			
	GLU273	39.5118	55.7814	52.8914	23.607	27.967	21.598	32.9746	53.9521	41.9441	24.098	26.536	**18.631**
	SER416	40.0773	43.4014	46.3464				40.5509	44.5579	46.8919			
Mu2	SER197	34.8646	53.3739	43.2989				34.4136	55.8615	42.914			
	GLU273	39.5289	55.96	52.72	23.475	28.096	21.497	38.7612	57.8684	50.3284	27.693	25.432	
	SER416	40.066	43.4997	46.1847				42.3411	45.9365	47.8501			**17.591**
Mu3	SER197	34.7446	53.1288	43.5638				34.7765	55.0284	41.6719			
	GLU273	39.4177	55.7358	52.7608	23.124	27.63	21.126	38.4333	56.9755	49.47	27.692	25.431	**17.591**
	SER416	39.9268	43.4407	46.4107				42.6536	45.2546	46.9906			

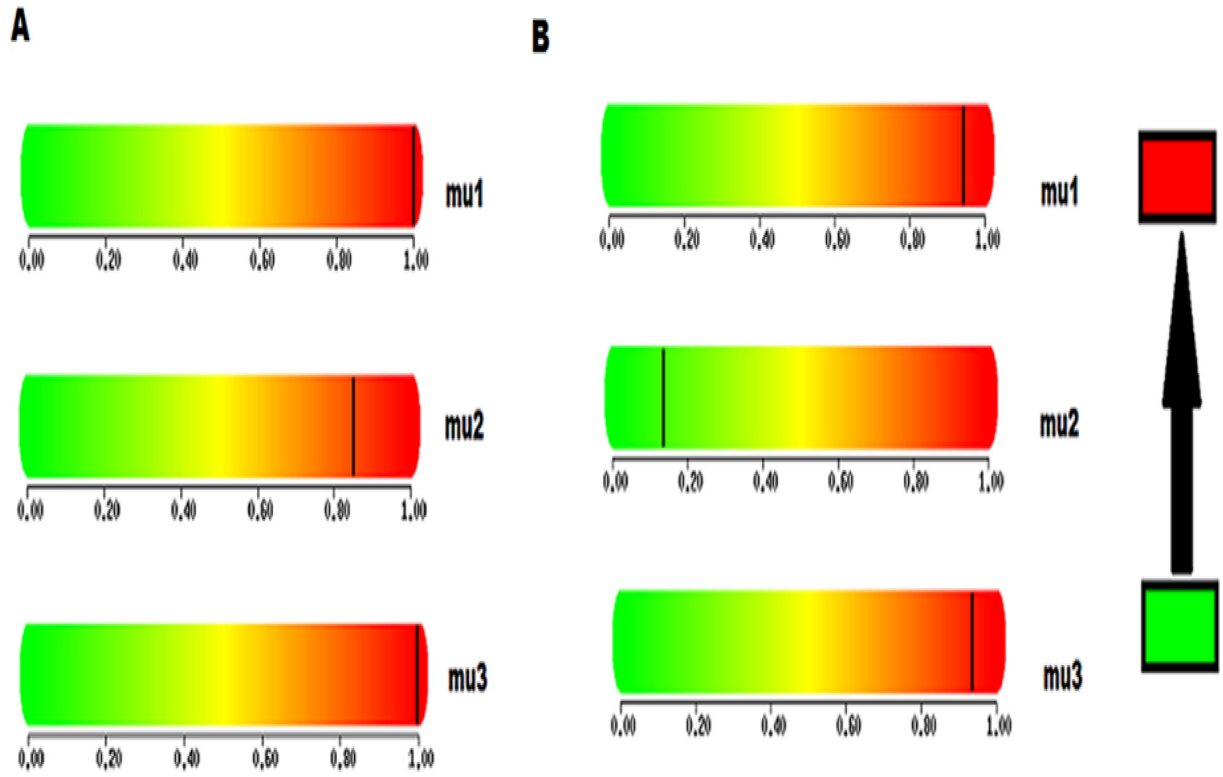

Fig. 4. (A) HumDiv (a preferred model for evaluating rare alleles) of PolyPhen2 (Polymorphism Phenotyping v2) predicted all the mutation to be PROBABLY DAMAGING, R155C is the most damaging of the three with a score of 1 (sensitivity: 0.00; specificity: 1.00) (B) HumVar (a preferred model for diagnostic of Medalian Disease) of PolyPhen2 predicted R155C and R155P to be PROBABLY DAMAGING and R155H as BENIGN with a score of 0.135 (sensitivity: 0.90; specificity: 0.71).

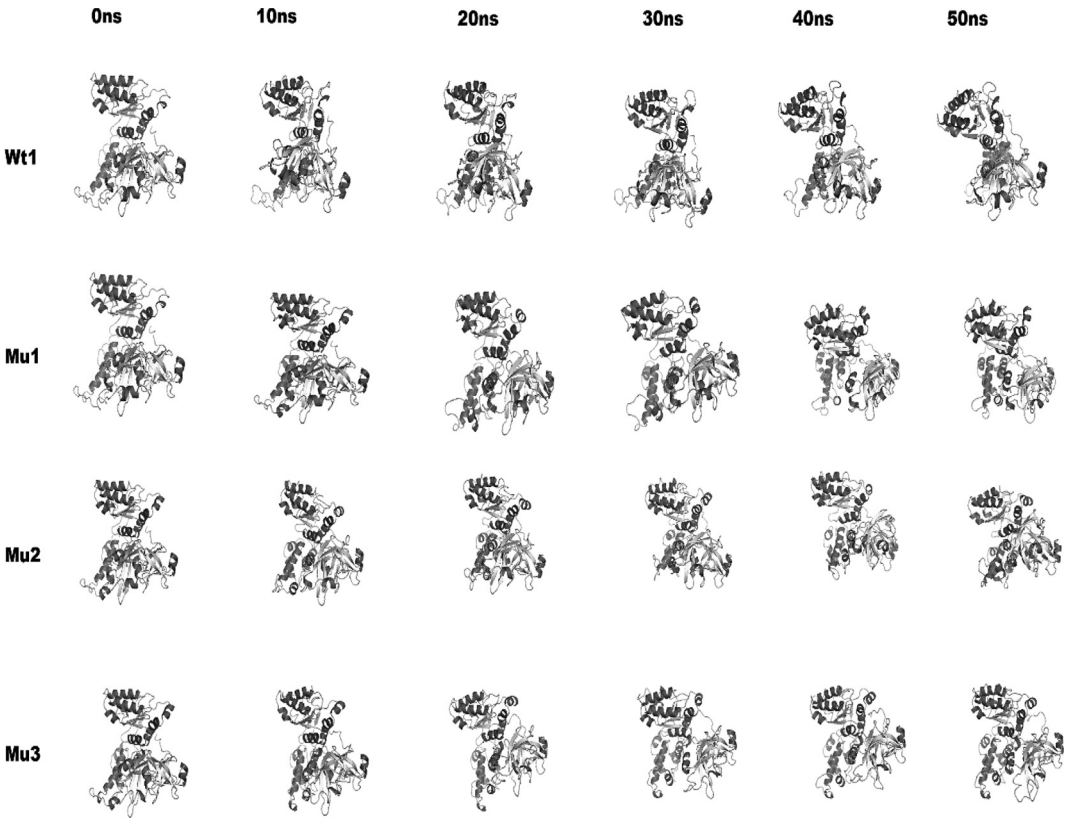

Fig. 5. Retrieved snapshots of the tertiary Wt, Mu1, Mu2 and Mu3 structures along 50 ns MDS trajectory, 10 ns gap was kept between each structure from left to right.

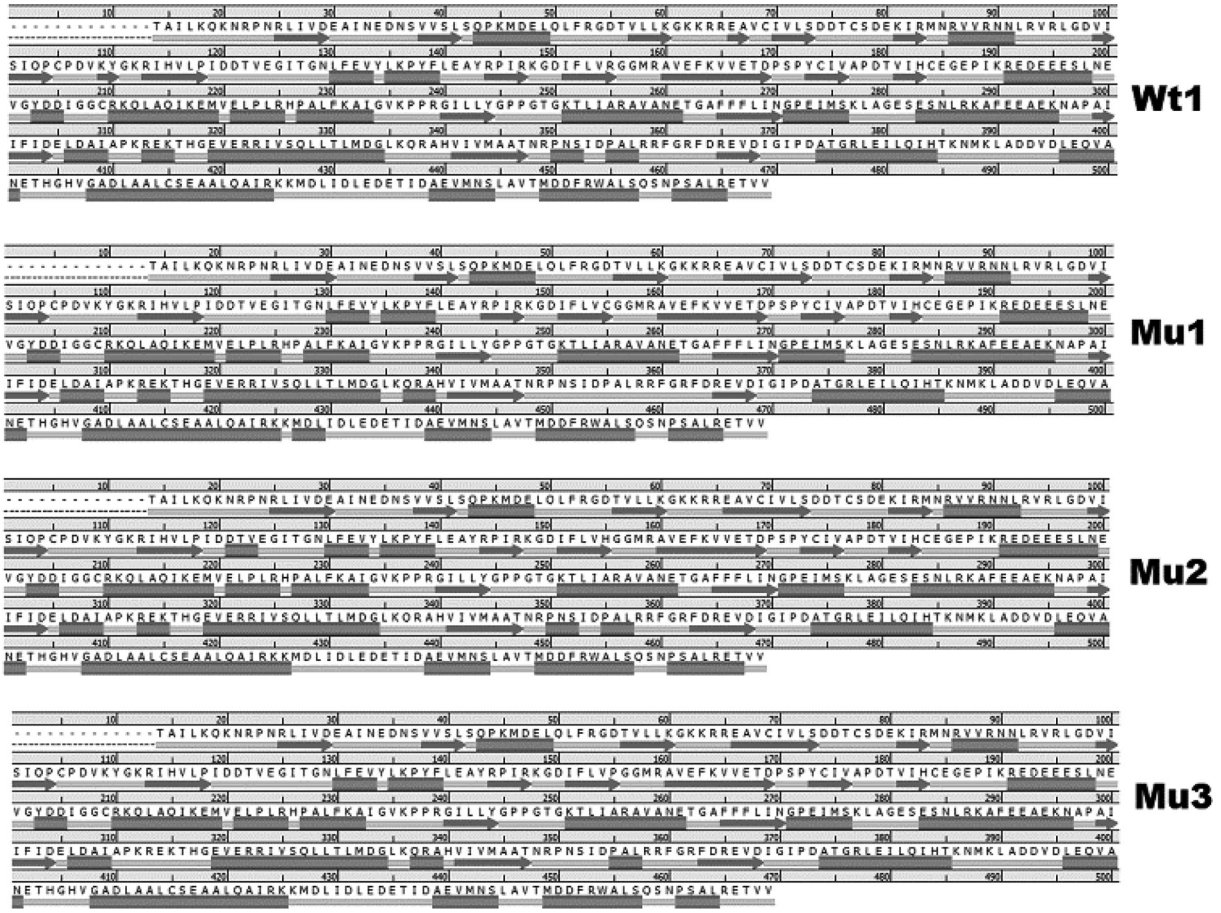

Fig. 6. Secondary structure layout of Wt, Mu1, Mu2 and Mu3 structures structures. Mu1 structure is showing maximum variation in secoundry structure elements when compared with that of Wt.

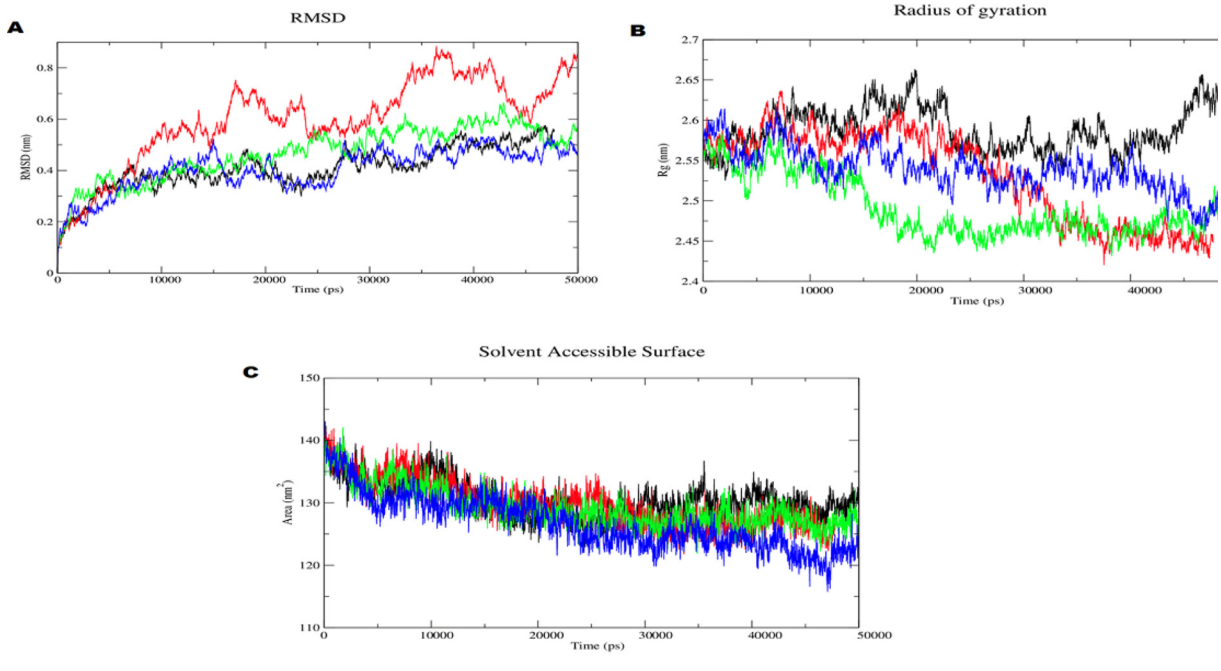

Fig. 7. (A) VCP's RMSD plot for wt (black) and Mu1 (red), Mu3 (green) and Mu4 (blue) structures at 310 K. The R155C structure is showing maximum deviation. (B) VCP's Radii of gyration for wt (black) and Mu1 (red), Mu3 (green) and Mu4 (blue) structures at 310 K. The R155C structure is showing maximum decrease over time. (C) VCP's Solvent Accessible Surface Area for wt (black) and Mu1 (red), Mu3 (green) and Mu4 (blue) structures at 310 K.

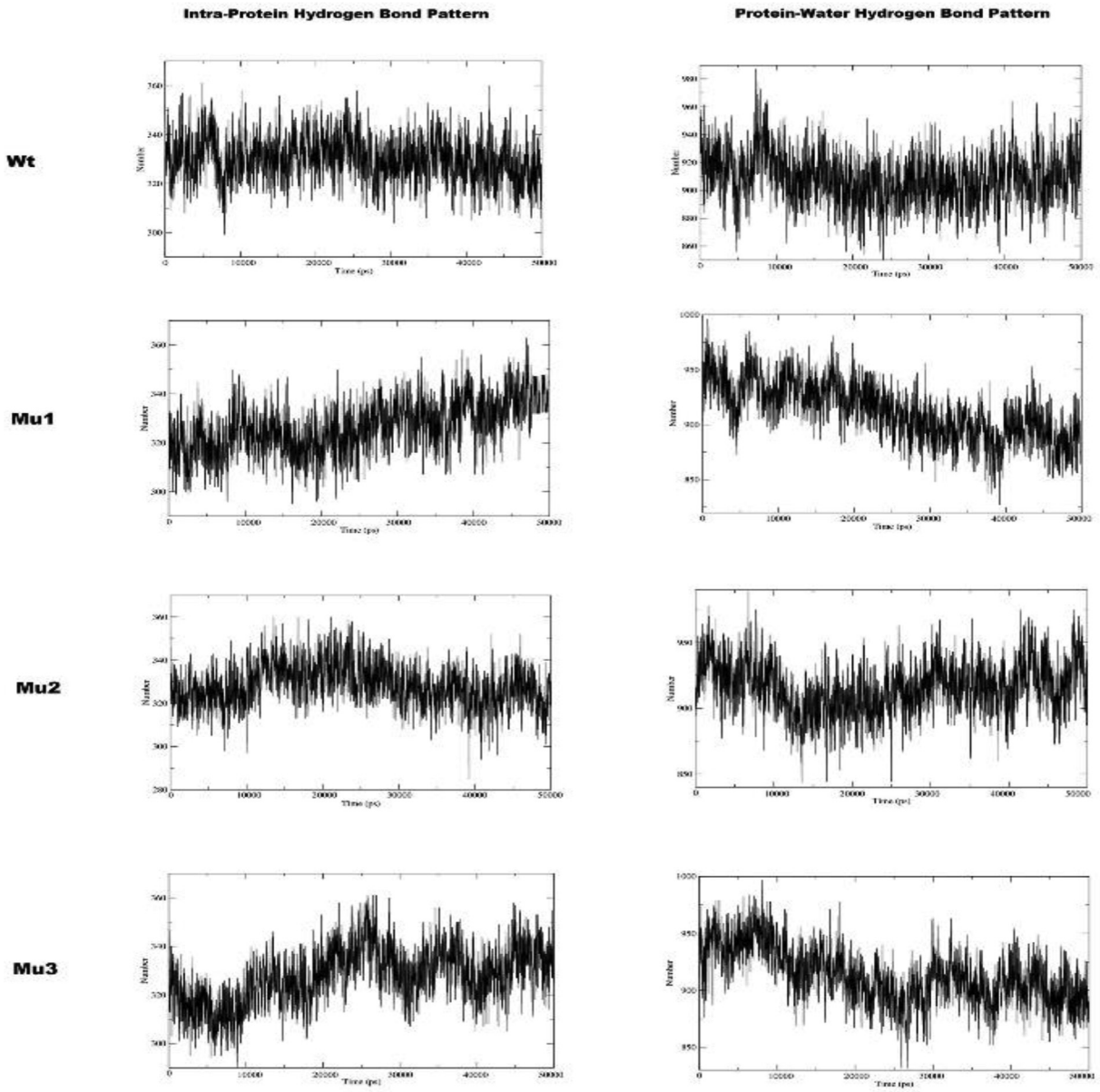

Fig. 8. Intra protein and protein-water hydrogen bond profile of the four structures of VCP over 50 ns time at 310 K.

under observation (blue representing the most stable and red most fluctuating). Fig. 9(D) shows the B factor projection where blue colour represents rigid and red represents most flexible, the mutant structures are showing significant fluctuations in N-terminal and D1-Domain. The comparative B factor projection primarily indicates fluctuations variations are most in R155C variant (see Figs. 10–12).

4. Discussion

The functional consequence of the three mutations reported at the VCP codon was studied. ATP–ADP transition was calculated, AutoDock tool was used to place the ATP and ADP in ATP/ADP binding domain (Baker et al., 2006). The ATP and ADP structures were docked in the D1-domain of the energy minimised four structures, the binding domain, the ATP/ADP transition were studied. The allosteric effect identified by this method showed that the mutations have a direct effect on ATP-ADP transition, and that the R155C variant was the most affected among three, having the maximum number of unfavourable interactions with ATP and ADP. The ATP/ADP binding mode was also studied in the available X-ray crystallographic structure of codon 155 mutant variant with ATP (4KO8) and ADP (4kod) in their binding pocket. The unfavourable interactions were also observed in their ATP/ADP binding pockets (Hooft et al., 1996). GLY408 appeared to be in all mutant ATP/ADP binding pockets, and was also observed in the ATP/ADP binding pockets of 4k08 and 4kod structure respectively. To study the changes in ATP/ADP binding grove, the distances between D1 ATPase domain, Dα domain and N-terminal were studied. Three amino acids GLU273, SER416 and SER 197 each from D1 ATPase domain, Dα domain and N-terminal respectively were selected for gauging their distance over time (Turner, 2005). The xyz coordination of the amino acids and the distance between them was analyzed. The major changes are observed in the distance between SER416 and SER197, where in the starting structures at 0 ns of wt, mu1 mu2, and mu3 the distance is around 21 Angstrom and at 50 ns the wt shows the distance at 33 Angstrom and all the mutants have around 18 Angstrom. This when observed at atomic level shows the conformational change is one of the helix of Dα domain of VCP. This data show that the wt structure at the end of 50 ns simulation shows a relaxed form attains an open confor-

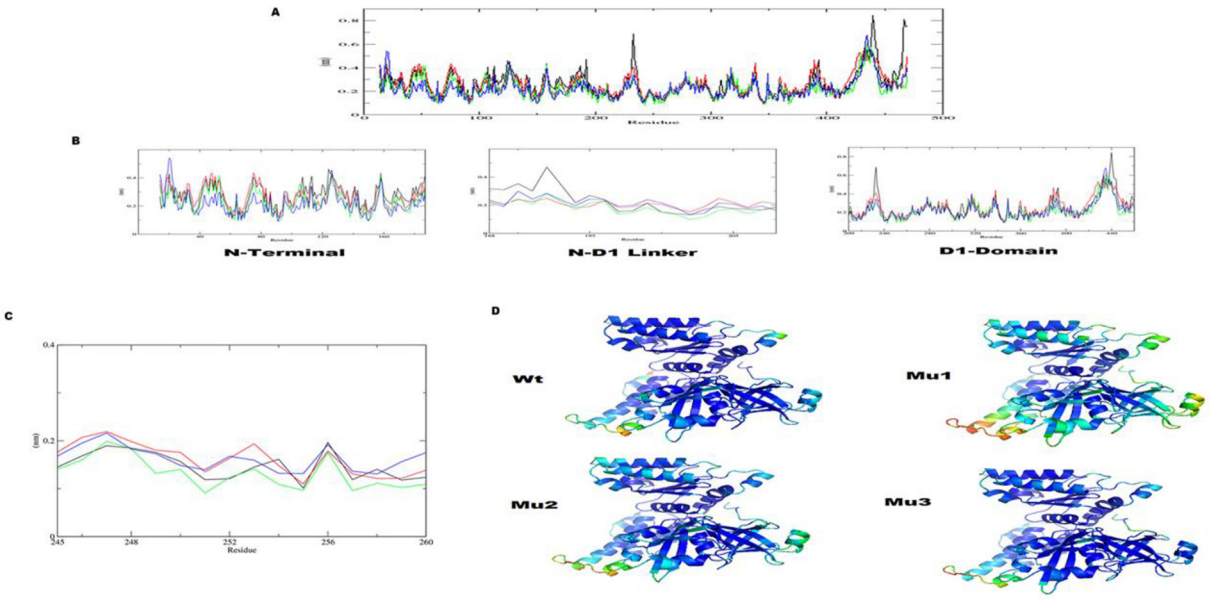

Fig. 9. (A) VCP residue RMSF at 310 K temperature of the four structures. (B) The domain based; N-Terminal, N-D1 liker and D1-domins RMSF profile at residue level of VCP and its 155 codon variants. (C) RMSF variation at the ATP binding domain of VCP, showing fluctuations across all amino acids in this domain. (D) Average Tertiary structures colored according to Bfactor values, Showing Mu1 to be most fluctuating.

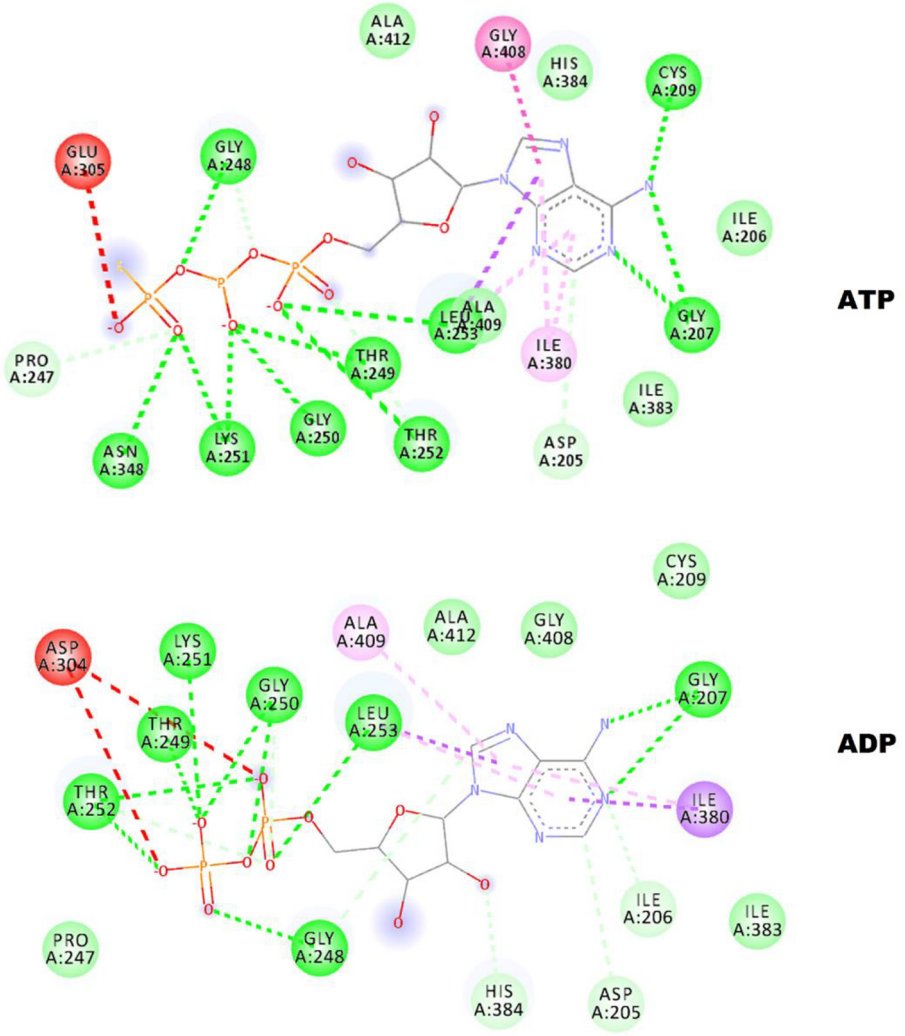

Fig. 10. ATP/ADP binding mode in valosin-containing protein (VCP), harbouring R155H mutation, the crystal structures used PDB ID: 4KO8 and 4KOD are co-crystallized with ATP and ADP respectively. The unfavourable interactions and the presence of GLY408 in the binding pocket are a common feature in these crystallized structures and our modelled mutant variants of VCP.

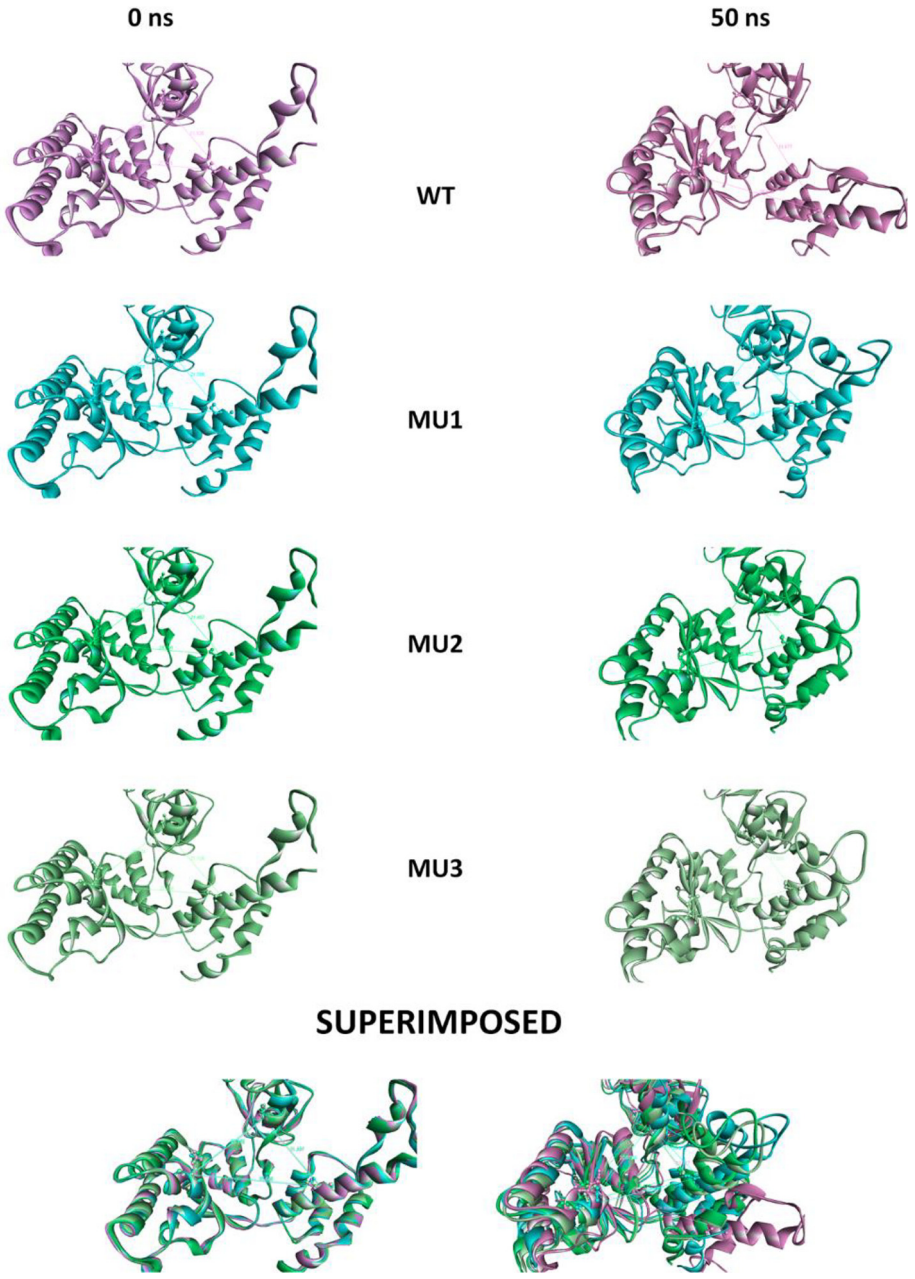

Fig. 11. Comparison of distance spanning through ATP/ADP binding domain of valosin containing protein (VCP).

mation, which is favorable for ATP/ADP transition (Dehouck et al., 2011). The data also affirms the movement of GLY 408 into the ATP/ADP binding pocket. The helix (400–425 amino acid) moves laterally relatively closer to the ATP/ADP binding pocket in all the mutant structures, the maximum shown by mu1. MM-PBSA calculations were employed to evaluate the binding free energy of ATP/ADP with VCP protein (Baker et al., 2006). The binding energies of the simulated complexes show that the ADP/ATP transition in R155C variant was affected the most. ATP showed the least binding of −163.901 (+/- 32.714) kJ/mol with R155C and the difference between ATP and ADP binding also least in this variant. These changes can alter the functioning of VCP (Tang and Xia, 2016).

5. Conclusions

Incongruities in ATP binding domain of any kinase enzyme and disease aetiology are synonyms. The occurrence of the mutation in protein like VCP is a contributing factor to a clinical multiple-disorder condition known as IBMPFD. Mutation at codon 155, a known mutational hotspot in VCP protein is an important factor that could impair ATPase activity of the D1-domain by affecting D1-D2 linker, the linker is capable of inducing asymmetry in subunit association into a VCP hexamer. The effect of D1-D2 linker on the ATPase activity of the D1-domain is already known and a significant genetic polymorphism in VCP will have an effect on its ATPase activity. As none of the studies till date has reported molecular dynamics simulation analysis of mutation in codon 155 of VCP, it has primarily prompted us to look into the possibility of computationally analysing of ATP/ADP transition. The structural transitions observed in secondary structure elements show that R155C mutant is showing the maximum variations, a factor that could influence ATP/ADP transition. The Rg of R155C mutant also shows that the structure is showing maximum deviation from Wt, the change can hamper VCP hexameric assembly. The conformational variability of D1-domain prompted us to look into ATP/

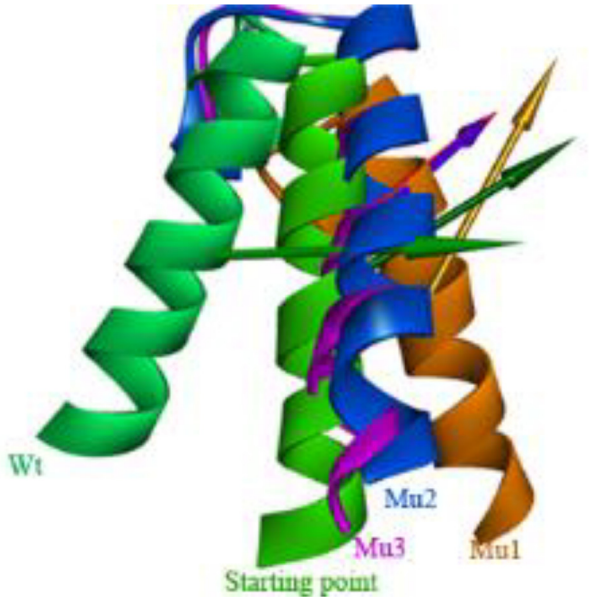

Fig. 12. The moment of the helix in Dα sub-domain of valosin-containing protein (VCP), where the starting point of all the structures is compared with 50 ns variant. The change in the moment of Wt with those of mutant structures is evident.

ADP transition kinetics. The molecular docking and MM-PBSA calculations reveal that ATP/ADP, despite binding to the same binding pocket shows a varying pattern in ATP/ADP-binding affinity coefficient. The analysis of the effect of mutations (R155C/ R155H/ R155P) using molecular dynamics simulation reveal the change in the secondary structure architecture, the change in intra-hydrogen bond pattern and ATP-ADP transition as major factors that presumptuously act as trigger for the onset of IBMPFD

Declaration of Competing Interest

The authors declare that they have no known competing financial interests or personal relationships that could have appeared to influence the work reported in this paper.

References

Adzhubei, I.A., Schmidt, S., Peshkin, L., et al., 2010. A method and server for predicting damaging missense mutations. Nat. Method. 7, 248–249.
Baker, M., Mackenzie, I.R., Pickering-Brown, S.M., et al., 2006. Mutations in progranulin cause tau-negative frontotemporal dementia linked to chromosome 17. Nature 442, 916–919.
Berendsen, H.J., Postma, Jv, van Gunsteren, W.F., DiNola, A., Haak, J., 1984. Molecular dynamics with coupling to an external bath. J. Chem. Phys. 81, 3684–3690.
Dehouck, Y., Kwasigroch, J.M., Gilis, D., Rooman, M., 2011. PoPMuSiC 2.1: a web server for the estimation of protein stability changes upon mutation and sequence optimality. BMC Bioinformat. 12, 151.
DeLano, W.L., 2002. The PyMOL molecular graphics system.
Elber, R., Ruymgaart, A.P., Hess, B., 2011. SHAKE parallelization. Eur. Phys. J. Special Topic. 200, 211–223.
Goodsell, D.S., Morris, G.M., Olson, A.J., 1996. Automated docking of flexible ligands: applications of AutoDock. J. Mol. Recog. 9, 1–5.
Guyant-Marechal, L., Laquerriere, A., Duyckaerts, C., et al., 2006. Valosin-containing protein gene mutations Clinical and neuropathologic features. Neurology 67, 644–651.
Haubenberger, D., Bittner, R., Rauch-Shorny, S., et al., 2005. Inclusion body myopathy and Paget disease is linked to a novel mutation in the VCP gene. Neurology 65, 1304–1305.
Hetzer, M., Meyer, H.H., Walther, T.C., Bilbao-Cortes, D., Warren, G., Mattaj, I.W., 2001. Distinct AAA-ATPase p97 complexes function in discrete steps of nuclear assembly. Nat. Cell Biol. 3, 1086–1091.
Hooft, R.W., Sander, C., Scharf, M., Vriend, G., 1996. The PDBFINDER database: a summary of PDB, DSSP and HSSP information with added value. Comp. Appl. Biosci. 12, 525–529.
Jorgensen, W.L., Chandrasekhar, J., Madura, J.D., Impey, R.W., Klein, M.L., 1983. Comparison of simple potential functions for simulating liquid water. J. Chem. Phys. 79, 926–935.
Kabashi, E., Valdmanis, P.N., Dion, P., et al., 2008. TARDBP mutations in individuals with sporadic and familial amyotrophic lateral sclerosis. Nat. Genet. 40, 572–574.
Kimonis, V., Donkervoort, S., Watts, G., 2018. Inclusion body myopathy with Paget disease of bone and/or frontotemporal dementia.In: Adam, M.P., Ardinger, H.H., Pagon, R.A., Wallace, S.E., Bean, L.J.H., Stephens, K., Amemiya, A., (Eds.), GeneReviews. University of Washington, Seattle, Seattle (WA); 1993–2018.
Kimonis, V.E., Fulchiero, E., Vesa, J., Watts, G., 2008. VCP disease associated with myopathy, Paget disease of bone and frontotemporal dementia: review of a unique disorder. Biochim. Biophys. Acta (BBA)-Mol. Basis Dis. 1782, 744–748.
Kondo, H., Rabouille, C., Newman, R., et al., 1997. p47 is a cofactor for p97-mediated membrane fusion. Nature 388, 75–78.
Kovach, M.J., Waggoner, B., Leal, S.M., et al., 2001. Clinical delineation and localization to chromosome 9p13.3-p12 of a unique dominant disorder in four families: hereditary inclusion body myopathy, Paget disease of bone, and frontotemporal dementia. Mol. Genetics Metabol. 74, 458–475.
Kumar, P., Henikoff, S., Ng, P.C., 2009. Predicting the effects of coding non-synonymous variants on protein function using the SIFT algorithm. Nat. Protocol. 4, 1073–1081.
Lowe, J., Spillantini, M.G., 1998. Non-Alzheimer Degenerative Dementias. Brain Pathol. 8, 295–297.
Lynch, T., Sano, M., Marder, K., et al., 1994. Clinical characteristics of a family with chromosome 17-linked disinhibition-dementia-parkinsonism-amyotrophy complex. Neurology, 44, 1878–1878.
Martoňák, R., Laio, A., Parrinello, M., 2003. Predicting crystal structures: The Parrinello-Rahman method revisited. Phy. Rev. Lett. 90, (7) 075503.
Mokhdomi, T.A., Bukhari, S., Chikan, N.A., et al., 2016. A novel kinase mutation in VEGFR-1 predisposes its αC-helix/activation loop towards allosteric activation: Atomic insights from protein simulation. Eur. J. Human Genetic. 24 (9), 1287–1293.
Neumann, M., Mackenzie, I.R., Cairns, N.J., et al., 2007. TDP-43 in the ubiquitin pathology of frontotemporal dementia with VCP gene mutations. J. Neuropathol. Exp. Neurol. 66, 152–157.
Pronk, S., Páll, S., Schulz, R., et al., 2013. GROMACS 4.5: a high-throughput and highly parallel open source molecular simulation toolkit. Bioinformatics 29 (7), 845–854.
Rabouille, C., Kondo, H., Newman, R., Hui, N., Freemont, P., Warren, G., 1998. Syntaxin 5 is a common component of the NSF-and p97-mediated reassembly pathways of Golgi cisternae from mitotic Golgi fragments in vitro. Cell 92, 603–610.
Racine, J., 2006. gnuplot 4.0: a portable interactive plotting utility. J. Appl. Econometric. 21, 133–141.
Rascovsky, K., Hodges, J.R., Knopman, D., et al., 2011. Sensitivity of revised diagnostic criteria for the behavioural variant of frontotemporal dementia. Brain 134, 2456–2477.
Ratnavalli, E., Brayne, C., Dawson, K., Hodges, J.R., 2002. The prevalence of frontotemporal dementia. Neurology 58, 1615–1621.
Skibinski, G., Parkinson, N.J., Brown, J.M., et al., 2005. Mutations in the endosomal ESCRTIII-complex subunit CHMP2B in frontotemporal dementia. Nat. Genetics 37, 806–808.
Studio D: Accelrys Inc. San Diego, CA, USA 2013.
Tang, W.K., Xia, D., 2013. Altered intersubunit communication is the molecular basis for functional defects of pathogenic p97 mutants. J. Biol. Chem. 288, 36624–36635.
Tang, W.K., Xia, D., 2016. Role of the D1–D2 Linker of Human VCP/p97 in the Asymmetry and ATPase Activity of the D1-domain. Sci. Rep. 6, 20037.
Turner, P., 2005. XMGRACE, Version 5.1. 19. Center for Coastal and Land-Margin Research, Oregon Graduate Institute of Science and Technology, Beaverton, OR.
Van Swieten, J.C., Heutink, P., 2008. Mutations in progranulin (GRN) within the spectrum of clinical and pathological phenotypes of frontotemporal dementia. Lancet Neurol. 7, 965–974.
Viassolo, V., Previtali, S., Schiatti, E., et al., 2008. Inclusion body myopathy, Paget's disease of the bone and frontotemporal dementia: recurrence of the VCP R155H mutation in an Italian family and implications for genetic counselling. Clin. Genetics 74, 54–60.
Wang, Q., Song, C., Li, C.-C.H., 2004. Molecular perspectives on p97–VCP: progress in understanding its structure and diverse biological functions. J. Struct. Biol. 146, 44–57.
Watts, G.D., Wymer, J., Kovach, M.J., et al., 2004. Inclusion body myopathy associated with Paget disease of bone and frontotemporal dementia is caused by mutant valosin-containing protein. Nat. Genetics, 36, 377–381.

Further Reading

George, D., Chakraborty, C., Haneef, S., NagaSundaram, N., Chen, L., Zhu, H., 2014. Evolution-and structure-based computational strategy reveals the impact of deleterious missense mutations on MODY 2 (maturity-onset diabetes of the young, type 2). Theranostics 4 (4), 366–385.
Kumari, R., Kumar, R., Lynn, A., 2014. g_mmpbsa A GROMACS Tool for High-Throughput MM-PBSA Calculations. J. Chem. Info. Model. 54, 1951–1962.
Laskowski, R.A., Swindells, M.B., 2011. LigPlot+: multiple ligand–protein interaction diagrams for drug discovery. J. Chem. Info. Model. 51, 2778–2786.